

## Article

# Unified Simplified Capacity Model for Beam-Column Joints into RC Moment Resisting Frame

Giancarlo Ramaglia <sup>1,2</sup>, Gian Piero Lignola <sup>1,\*</sup> , Francesco Fabbrocino <sup>2</sup>  and Andrea Prota <sup>1</sup>

<sup>1</sup> Department of Structures for Engineering and Architecture, University of Naples Federico II, Via Claudio 21, 80125 Naples, Italy

<sup>2</sup> Department of Engineering, Telematic University Pegaso, Piazza Trieste e Trento, 48, 80132 Naples, Italy

\* Correspondence: [gignola@unina.it](mailto:gignola@unina.it)

**Abstract:** Seismic vulnerability of reinforced concrete (RC) buildings is strongly influenced by beam-column joints. Horizontal and vertical structural members converge in beam-column joints, as extremely delimited areas where the internal forces in concrete core and reinforcing bars have elevated stress gradients. In order to fully understand the seismic behavior of RC buildings and the related failures of T- and X-shaped beam-column joints (external corner and internal-positioned), an analytical model of RC joint behavior is proposed in a unified and simplified way. The equilibrium equations of cracked joint portions allow the assessment of internal stresses' evolution at increasing values of column shear forces. In this way, the strength hierarchy is evaluated in terms of capacity for the different potential failure modes. This can drive, as a useful tool for designers, the design of new efficient structures or the assessment of existing ones to occur, with subsequent interventions to move an initial undesired failure mode to a more suitable one. Nearly 500 experimental results of tests available in the literature are compared with the analytical predictions of the proposed model.

**Keywords:** simplified model; RC joints; strength hierarchy



**Citation:** Ramaglia, G.; Lignola, G.P.; Fabbrocino, F.; Prota, A. Unified Simplified Capacity Model for Beam-Column Joints into RC Moment Resisting Frame. *Appl. Sci.* **2022**, *12*, 10709. <https://doi.org/10.3390/app122110709>

Academic Editor: Omar AlShawa

Received: 3 October 2022

Accepted: 18 October 2022

Published: 22 October 2022

**Publisher's Note:** MDPI stays neutral with regard to jurisdictional claims in published maps and institutional affiliations.



**Copyright:** © 2022 by the authors. Licensee MDPI, Basel, Switzerland. This article is an open access article distributed under the terms and conditions of the Creative Commons Attribution (CC BY) license (<https://creativecommons.org/licenses/by/4.0/>).

## 1. Introduction

The structural behavior of beam-column joints represents a key aspect for both new and existing reinforced concrete (RC) buildings. Recent seismic events have shown the fragility of these components in existing RC buildings. Therefore, the beam-column joint must be accurately designed into RC moment resisting frames. Many existing buildings were constructed at a time when no anti-seismic regulations [1,2] were available, making them strongly vulnerable under seismic actions [3–5]. Beam-column joints in RC buildings are circumscribed portions where high loads transfer between the connecting beams and columns. In fact, the internal stresses increase due to local effects, which govern the equilibrium of beam-column joints [6,7]. This aspect becomes strongly crucial in the seismically resistant frames, where the post-elastic capacity of RC members (non-linear effects) is mobilized due to the large demand [8,9]. The major dissipation could be concentrated in these portions, promoting brittle failure modes when the RC joints are poorly designed. This phenomenon appears to be very recurrent in existing RC buildings, jeopardizing the strength resources of entire structures [10,11]. For this reason, the modern building codes [1,2,12] pay close attention to the design of these structural components. In fact, in the new buildings, they shall be correctly designed [13,14] in order not to activate brittle failure modes [15–17].

Under dynamic actions, the failure mode of beam-column joints is governed by two main mechanisms: debonding and shear failure mechanisms, which are generally brittle [18–20]. RC joints can be modeled in general as bidimensional elements [21,22]; however, this approach has some drawbacks, especially in the numerical modeling [23,24]. When a beam-column joint is subjected to seismic action [25,26], the beams connecting into the joint are subjected

to a bending moment in the same direction. The steel bars of the same layer at opposite sides of the RC joint panel are pulled or pushed in the same load direction [27,28]. The internal stresses strongly increase due to these local effects [29,30]. When the strengths of materials (concrete and steel) are lower than the imposed stresses, the equilibrium condition cannot be guaranteed, and the RC joint cracks and collapses [31,32]. The beams could lose their load capacity if the steel bars slip inside the joint region. Furthermore, the cyclic load provides diagonal pull and push actions, and the concrete joint panel diagonally cracks [33,34]. For this reason, the stirrups provide a beneficial effect on the ultimate behavior of the RC joint [35–37]. The shear strength and the passive confinement effect increase the load capacity of the RC joint panel, preserving the RC joint from a premature brittle failure mode. According to the modern building codes, a proper amount of stirrups allows the internal stresses to be properly transferred between the main structural elements (converging beams and columns). Unfortunately, the existing building stock shows a deficiency of stirrups in joint panels, due to the old design criteria often being based on gravitational condition only [38,39].

The current research aims to develop cost-effective strengthening strategies [40,41] by means of ordinary and innovative techniques [42–44]. Ordinary strengthening systems, namely steel or RC jackets, have been largely studied in the past [45,46]. The benefits of several innovative materials, if compared with the past systems, were shown in several scientific works [47,48]. These systems have been largely applied in engineering practice due to many benefits: mechanical performance, light weight, corrosion resistance, and very fast constructability [49,50]. The efficiency in terms of structural capacity of RC joints has been experimentally demonstrated [51,52]. Strengthening based on fiber-reinforced polymer (FRP) or fiber-reinforced cementitious matrix (FRCM) [53–59] can be used to improve the structural capacity of RC joints. The best strategy depends significantly on the mechanical performance of the concrete support [60,61]. Furthermore, these systems allow the application of local structural improvements without changing the global behavior [62,63]. In particular, they can be used to improve the structural capacity without modifying the stiffness [64,65].

The behavior of unreinforced and strengthened RC joints is a crucial aspect, especially from a designer point of view. Semi-empirical approaches to designing new RC joints are provided by recent building codes. Traditional strut and tie or truss models to predict the shear strength mechanism offer some drawbacks, especially for existing structures, as demonstrated in many scientific works [66–69]. These are based on laboratory testing and, therefore, are characterized by limited applicability. Furthermore, these models neglect the impact of other key factors, such as the extent of the axial load or the flexural capacity of the members converging in the RC joint. Some studies have provided first efforts to identify the main key factors by means of a mechanical model [70,71]. They constitute the basis of the improvements provided by the proposed model. Starting from the existing experimental results, it has been observed that the joint failure is not always due to an exceedance of joint shear stress capacity. This aspect is due to a particular phenomenon which has been experimentally observed (i.e., joint shear stress and story shear do not reduce equally during experimental tests [72]).

A recent study [73] proposed an improved non-linear model for beam-column RC joints with additional calibrations. This model includes the influence of joints on seismic performance of RC frames in numerical analyses with their deformability, including several failure modes, such as the bond-slip behavior. Further studies [74] implementing this model on more complex structures (Finite Element Models (FEM)) have clarified many key factors in the behavior of beam-column RC joints. Other non-linear models based on rotational hinges have been refined [75], or macro-element models have been outlined [76], in order to simulate the ultimate behavior of the RC joints. However, this has led to complex and cumbersome FEM models, which are usually not acceptable for practitioners.

This topic boasts several available scientific works in the literature, as several beam-column joint models have been proposed. Many of them are essentially oriented to research

coupled with detailed and refined modeling of the structures. However, such models also have benefits and shortcomings; hence, there is definitely no wide consensus on which is the best modeling approach.

The present paper proposes a unified, simplified approach suitable for analyzing seismic-resisting frames and detecting beam-column RC joint failure, thus obtaining a balance between practicality and accuracy.

## 2. Research Significance

The goal of this work is to investigate the ultimate behavior of exterior and interior located RC beam-column joints by means of a generalized model. The present work represents an improvement on the simplified models introduced in [77,78], which deal with modeling X-shaped beam-column and T-shaped beam column joints, respectively, in RC frames.

First goal of this paper is to develop a unified model that allows for analysis of both types of RC joints. The ultimate state is evaluated to assess beam-column joints and their strength hierarchy at failure. The proposed approach conforms to strength hierarchy and capacity design principles, driving recent building codes. In fact, the behavior of beam-column RC joints impacts both the strength and ductility of entire structures. The proposed model can be used also to assess the efficiency of strengthening strategies and allows to change initial undesired failure modes to more suitable ones. The effect of strengthening systems can be easily implemented by using equivalent approaches.

Finally, the numerical results provided by the proposed model have been discussed and compared to a large set of about 500 experimental results on X-shaped and T-shaped beam column joints [79], confirming its predictability.

## 3. Analytical Model

The present study focuses on the behavior assessment of RC joints in moment resisting frames. In these structures, perimeteric and internal joints can be identified in the frame. The internal joints benefit from confinement of the beams coming to the sides of the vertical elements. In fact, according to the modern building codes [1,2,12], these RC joints could not be verified due to this beneficial effect. The perimeteric RC joints are more critical, because the confinement provided by the converging RC members is lower. The proposed analytical model can be used to assess both X-shaped and T-shaped beam column RC joints. The analytical model is based on knowledge of few key parameters.

Experimental programs [27,32,35] allowed for the assessment of the main parameters that govern the ultimate behavior of RC joints. The experimental joint database [79–81] indicates the typical failure modes of RC joints. The experimental programs refer to a significant number of RC joints with different geometries, assessing the (usually cyclic) load levels pushing the joint to failure. The failure mode can be due to several mechanisms strongly influenced by the geometrical and mechanical characteristics of RC joints:

- shear failure modes generally with or without the yielding of longitudinal reinforcement bars of beams;
- concrete cracking is generally linked to bond or yielding failure mode of longitudinal reinforcement bars of beams.

The effects of different mechanisms are also clear on the global force displacement capacity curves, where several mechanisms differently alter the stiffness. Starting from the existing, available literature [70,79], key parameters have been identified to develop the proposed simplified model. The main parameters that govern the behavior of the RC joint can be identified as:

- material properties;
- geometry of the RC joint panel;
- type of RC joint (X-shaped or T-shaped);
- reinforcement bars in the RC joint panel;
- axial load acting on the RC joint panel;

- bond condition of reinforcement;
- geometrical and mechanical properties of strengthening systems;
- shear and flexural capacity of the converging members (beams and columns), possibly coupled with strengthening systems.

The analytical model represents an improvement on the model proposed by Shiohara [82]. The proposed model provides a mathematical formulation applicable in the cases of X-shaped and T-shaped RC joints. For X-shaped RC joints, the symmetry allows for simplification of the numerical formulation. In particular, the direction of the seismic action does not influence the analytical formulations. For T-shaped RC joints, the mathematical formulation assumes different forms as the direction of the seismic action changes. This is due to the missing symmetry, which causes the capacity of T-shaped RC joints to depend on the direction of the beam and column shear. Starting from the parameters previously discussed, the shear applied to columns (namely, column shear) was considered to be the main parameter in a frame analysis. The proposed model was applied to several cases, and experimentally tested and related failure modes have been detected for each of them. The experimental data [79] refer to about 500 X-shaped and T-shaped RC joints. According to the experimental setup for each RC joint, some parameters have changed to assess the relevant changes in terms of failure modes and capacity.

### 3.1. Equilibrium Condition of the RC Joint

The mathematical formulation is based on internal equilibrium conditions, and it allows for the assessment of the failure mode under ultimate conditions. The direction of the seismic action alters the internal equilibrium conditions when the RC joint is characterized by a T-shape. In this paper, a unified mathematical formulation will be discussed. It allows the application of the proposed approach to RC joints of any shape (X and T type). According to modern guidelines [1,2,12], internal RC joints can also be analyzed by using a plane model once the main joint panel has been both mechanically and geometrically characterized.

The equilibrium conditions can be written for the T-shaped and X-shaped RC joint, once the geometrical characteristics and the internal forces are known. Figure 1a shows the case of T-shaped RC joints subjected to positive or negative column shear, respectively. The parameter  $\alpha$  represents the ratio between the length of the column and beams, called  $L_c$  and  $L_b$ , respectively. Conversely, the internal equilibrium condition is shown in Figure 2a,b as the direction of the seismic action changes. The main difference is clear in Figure 1b due to the symmetry of the internal stresses for the X-shaped RC joint, drawn with different colors in order to clarify the relevant longitudinal reinforcements depicted in the corresponding cross-sections, as well. Figure 2a,b show the two different directions of the column shear,  $V_c$ , due to the asymmetry of the T-shaped RC joint. In particular, the internal stresses acting in the RC joint change with the direction of the column shear. This effect does not occur for the X-shaped RC joint, as shown in Figure 2c. The depth of RC joint can be also different from the depth of the beam and column.

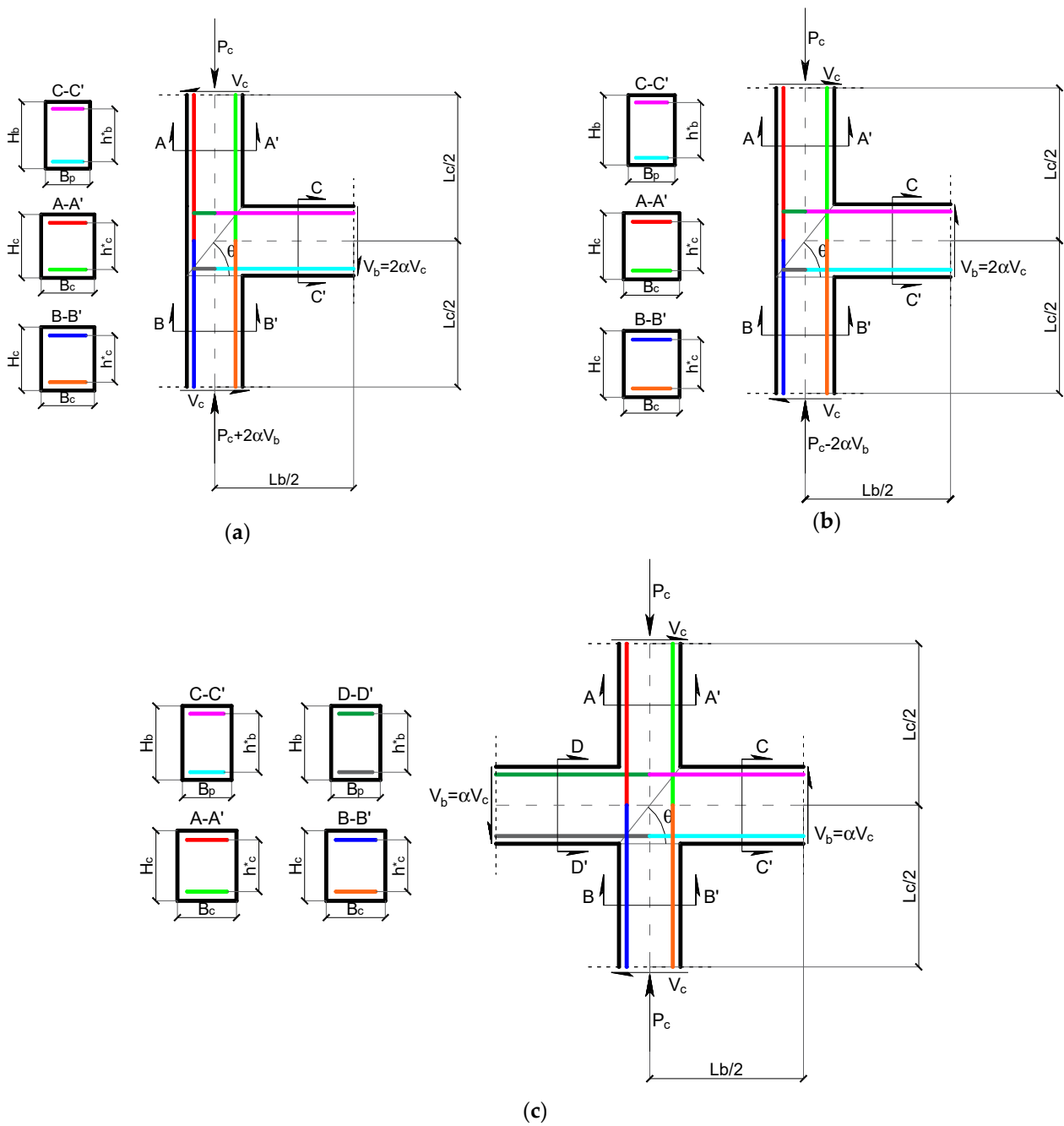


**Figure 1.** Characteristics and external forces acting on the RC joints: (a) positive direction of the column shear acting on the T-shaped RC joint, (b) negative direction of the column shear acting on the T-shaped RC joint, and (c) positive direction of the column shear acting on the X-shaped RC joint (negative is symmetrical).

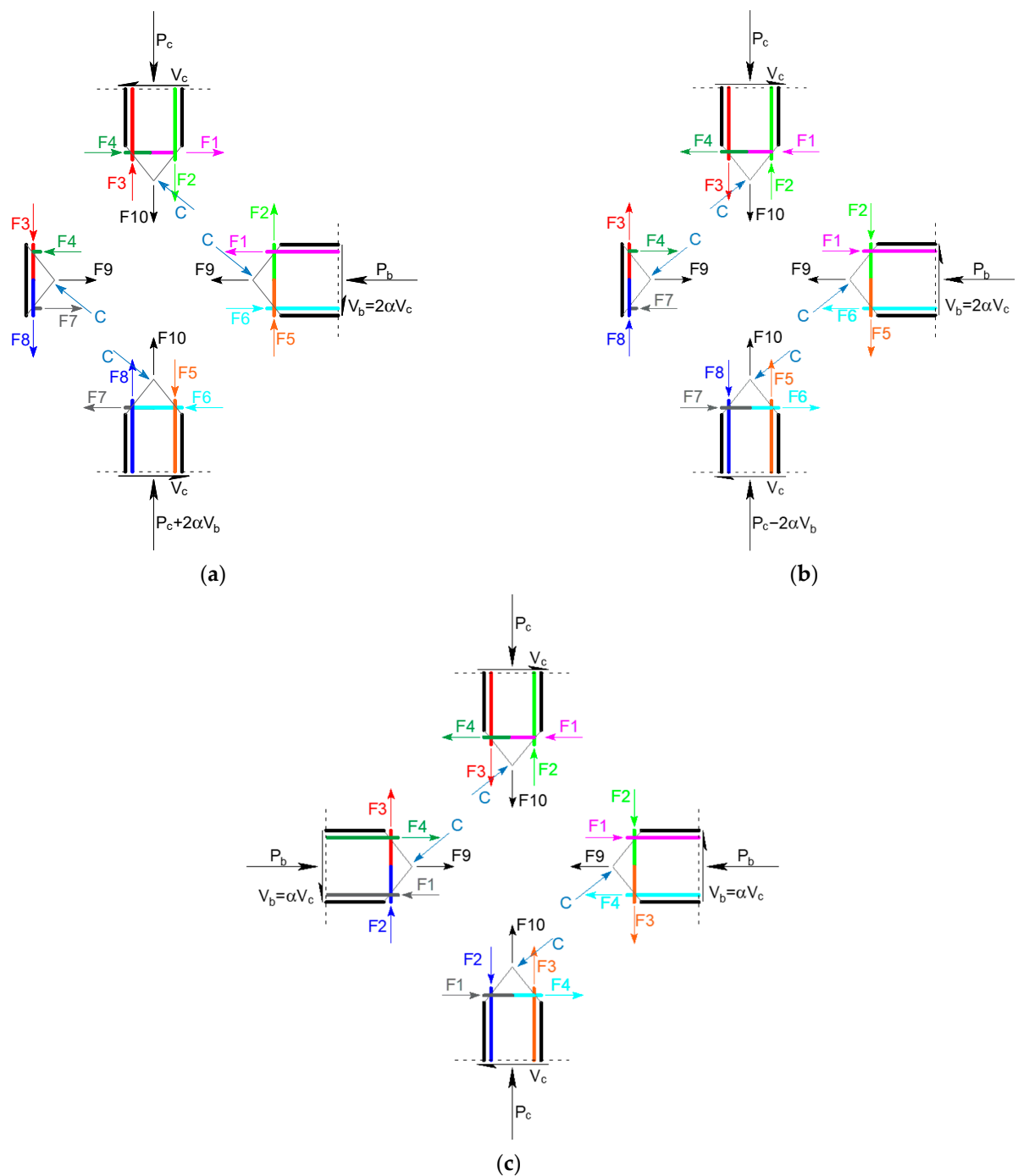


**Figure 2.** Internal equilibrium conditions for the RC joints: (a) positive direction of the column shear acting on the T-shaped RC joint, (b) negative direction of the column shear acting on the T-shaped RC joint, and (c) positive direction of the column shear acting on the X-shaped RC joint (negative is symmetrical).

The compressive force  $F_1$  is obtained by adding the contribution of the concrete  $C_i$  and the reinforcement  $S_i$  in compression, as shown in Figure 3.

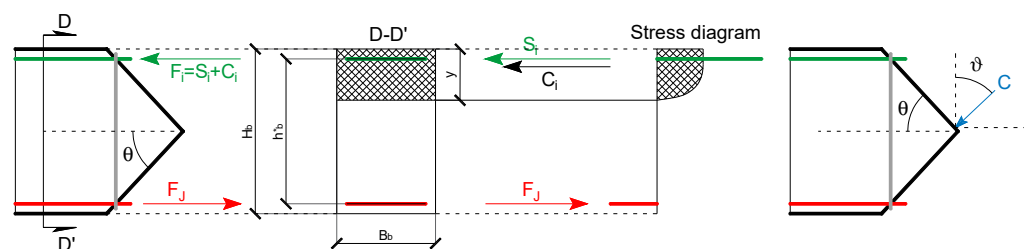


**Figure 3.** Analysis of compressive forces,  $F_i$ , components in concrete,  $C_i$ , reinforcement,  $S_i$ , and compressive forces,  $C$ , in joint core (inclination  $\theta$  for cracked portion and  $\vartheta$  for C).

The behavior of the RC joint panel is assessed by means of a discretized approach in cracked condition. In particular, the RC joint panel is modeled as four portions (i.e., rigid bodies) obtained by intersecting the two diagonals of the RC joint panel, each with an inclination  $\theta$ . Under a generic load, the RC joint is subjected to several internal forces (Figure 2). The internal forces are derived from the resultants of the internal stress acting on the longitudinal bars, stirrups, and compressed concrete. The contributions provided by the bars and concrete around compressed bars have been supposed to be applied at bars location. The contribution provided by the compressed concrete diagonal strut in the joint is modeled as a resultant force,  $C$ , acting on the boundary of each portion of the RC-joint panel. It has been supposed to act equally on each half of the diagonal of the RC joint panel. The inclination  $\vartheta$  of this resultant force depends on the internal stress distribution. However, it can be assumed to act normally to the crack (hence  $\vartheta = \theta$ ), and it is centered with respect to the diagonal of the RC joint.

Both for the T-shaped and the X-shaped RC joint, twelve equilibrium equations can be written to assess the ultimate behavior and the occurred failure mode. For the X-shaped RC joints, the equilibrium equations can be simplified, exploiting the symmetry. In particular, the number of independent equations is reduced to five, but the unknown terms are at least eight. Some of them could be fixed according to typical experimentally detected behavior [79] or directly assigned in the design phase.

However, in order not to fix a great number of unknown terms a priori (assumed at their maximum capacity or supported by experimental results), different solutions will be discussed to assess the failure modes as the input parameters change. Furthermore, the proposed model allows the inclusion of the RC converging members failure mode (beams and column) into a unified RC joint model. For this reason, a distinct check on the flexural (or shear) failure for beams and columns was added. These assumptions allow the merging of the concrete compression,  $C_i$ , and the steel compression,  $S_i$ , in a compression resultant only, acting at both beam and column ends (Figure 2). This simplification provides a negligible approximation on the equilibrium of beams and columns [83].

Furthermore, the proposed model allows the assessment of the potential failure mode due to the RC joint or the beam or the column. The capacity of the RC joint is the smallest of the capacities related to their failure modes.

Finally, the evolution of all other unknown terms can be assessed as the column shear increases up to the ultimate condition. In fact, the column shear is not an unknown parameter, but is the main input parameter. The evolution of other internal forces (unknown terms) depends on the column shear,  $V_c$ . It represents a key aspect, due to the compatibility with the modern basic capacity design principles [1,2,12]. In particular, the joint capacity, in terms of shear force, is provided for each failure mode.

The equilibrium configuration was fixed by setting the geometrical parameters and the internal stresses, as shown in Figure 2, for the T-shaped (Figure 2a,b) and the X-shaped (Figure 2c) RC joint.

For the T-shaped RC joint, under positive column shear,  $V_c$  (Figure 2a), the tensile resulting forces of longitudinal bars are named  $F_1$ ,  $F_2$ ,  $F_7$ , and  $F_8$ , while the compressive forces are  $F_3$ ,  $F_4$ ,  $F_5$ , and  $F_6$ . These internal forces cross the RC joint panel, as clarified in Figure 1a. The resultant forces provided by the stirrups and/or eventual strengthening

systems on the RC joint are named F9 and F10. Finally, C represents the compression resultant force of concrete acting on the RC joint panel. Several strengthening systems can be coupled with the existing reinforcement to provide an additional capacity [84,85]. In particular, F9 is the resultant force provided by steel stirrups or externally bonded reinforcement (EBR), placed horizontally. Conversely, F10 is the resultant force provided by EBR, placed vertically. These additional EBRs can be made of several classical or innovative materials. Therefore, the proposed model allows the assessment of the increases in capacity due to the strengthening systems.

When the column shear becomes negative (Figure 2b), the compressed resultants are named F1, F2, F7, and F8, while those in traction are named F3, F4, F5, and F6. F9, F10, and C have been previously defined.

The internal forces can be evaluated by solving a system of equations according to three degrees of freedom for each of the discretized portions (four rigid portions) of the RC joints. In particular, equilibrium equations on vertical and horizontal translations, as well as rotation, must be used. The equilibrium equations provide twelve equations, where only nine are independent. It is possible to reduce the unknown internal forces to nine once the internal forces F9, F10, Pb, and Pc are known. In particular, F9 and F10 are internal forces to be fixed, while Pc and Pb are the external axial forces applied to the upper column and beam, respectively, which are usually known parameters.

For the X-shaped RC joint, a single load direction of the seismic action can be analyzed. A load reversal provides a symmetrical stress state. The beam column joint is clearly symmetric if the joint is exactly at  $L_b/2$  and  $L_c/2$ . These geometrical characteristics are generally available in the experimental setup and in new RC joints. However, this does not mean that steel reinforcements have the same cross-section or full area to have an equal resultant. In particular, RC joints show a symmetry in terms of forces (internal and external) but not necessarily in terms of geometrical characteristics of reinforcement bars. The number of non-linear independent equations is five, in five unknowns (C, F1, F2, F3, and F4), due to the symmetry.

$$F_i = C_i + S_i \quad (1)$$

All internal forces can be evaluated as functions of the column shear,  $V_c$ , by solving the following system of equations, both for positive and negative column shear applied on T or X-shaped RC joints:

$$F_1 + F_4(1 - i) + F_6i - C \cdot \sin\theta - V_c = 0; \quad (2)$$

$$F_1 - F_6i + F_4(1 - i) + (F_9 - C \cdot \sin\theta + P_b) \frac{V_c}{|V_c|} i - (F_9 - C \cdot \sin\theta + P_b)(1 - i) = 0 \quad (3)$$

$$(F_4(1 - i) + F_6i + F_7 - C \cdot \sin\theta - V_c)i = 0; \quad (4)$$

$$(F_3(1 - i) + F_5i - F_2) \frac{V_c}{|V_c|} (i) - F_{10} + C \cdot \cos\theta - P_c - (F_3(1 - i) + F_5i - F_2)(1 - i) = 0; \quad (5)$$

$$F_2 + F_5i + F_3(1 - i) - C \cdot \cos\theta - (1 + i)\alpha \cdot V_c = 0; \quad (6)$$

$$\left( F_8 - F_3(1 - i) - F_5i + (F_{10} - C \cdot \cos\theta + P_c) \frac{V_c}{|V_c|} + 2\alpha \cdot V_c \right) i = 0; \quad (7)$$

$$h_b^*(F_1 + F_4(1 - i) + F_6i) + h_c^*(F_2 + F_3(1 - i) + F_5i) - \frac{C^2}{B \cdot f_c} - L_c \cdot V_c = 0; \quad (8)$$

$$\left( h_b^*(F_1 + F_4(1 - i) + F_6i) + h_c^*(F_2 + F_5) - \frac{C^2}{B \cdot f_c} - 2 \cdot L_c \cdot V_c \right) i = 0; \quad (9)$$

$$\left( h_b^*(F_1 + F_7) + h_c^*(F_3(1 - i) - F_5i + F_8) - \frac{C^2}{B \cdot f_c} - L_c \cdot V_c \right) i = 0. \quad (10)$$

In the previous equations,  $f_c$  represents the compressive strength of concrete, while  $\alpha$  is the aspect ratio  $L_c/L_b$ . Furthermore, in the previous equations, column shear, beam shear, and bending moments on beam and column ( $V_c$ ,  $V_b$ ,  $M_c$  and  $M_b$  respectively), also satisfy the following conditions, representing additional equations:

$$\left( V_c - \frac{V_b}{(2-i)\alpha} \right) = 0 \tag{11}$$

$$\left( V_c - \frac{2M_c}{L_c - H_b} \right) = 0 \tag{12}$$

$$\left( V_c - \frac{(2-i)M_b}{(L_b - H_c)\alpha} \right) = 0 \tag{13}$$

$$(V_b - 2\alpha \cdot V_c)i = 0 \tag{14}$$

The  $i$ -index allows the assessment of the structural behavior of any shape of the RC joint (T or X-shaped). Some internal forces, as shown in Figure 2, must be permuted when the shape shifts from T to X. Therefore, a generalized system of equations can be written in order to assess the behavior of any RC joints, by using the following math assumptions, and noting that identity  $0 = 0$  means that the equation is redundant for the purpose of solving the problem:

$$i = \begin{cases} 0 & \text{for X-shaped RC joints} \\ 1 & \text{for T-shaped RC joints} \end{cases} \tag{15}$$

The symbols shown in the previous equations are reported in the Figures 1 and 2, as well as in the notation list (Table 1). The width,  $B$ , of the RC joint can be identical to the width of the beams or column,  $B_b$  and  $B_c$ , respectively, or it can be different.

Once the previous system of equations is solved, each internal force can be correlated to column shear,  $V_c$ . This correlation allows for the estimation of the maximum value of the column shear, due to the first failure mode (an internal force reaches its threshold value). The ultimate condition, in fact, depends on the ultimate value of internal forces  $F_i$ . In particular, for each ultimate value of internal forces  $F_i$ , the correlated column shear,  $V_c$ , can be evaluated according to the failure modes outlined in Table 1. The actual capacity of the RC-joint is given by the minimum value among all column shear forces.

**Table 1.** Ultimate column shear,  $V_c$ , due to each linked failure mode.

Column Shear	Failure Mode
$V_{c1}$	Flexural capacity of beam (FSB)
$V_{c2}$	Flexural capacity of column (FSC)
$V_{c3}$	Shear capacity of beam (SSB)
$V_{c4}$	Shear capacity of column (SSC)
$V_{c5}$	Yielding of horizontal bottom (YBB) or top bars (YTB) in beams
$V_{c6}$	Yielding of vertical bars on the top column (YTC)
$V_{c7}$	Yielding of vertical bars on the bottom column (YBC)
$V_{c8}$	Maximum bond capacity exceedance (BC1)
$V_{c9}$	Average bond capacity exceedance (BC2)
$V_{c10}$	Minimum bond capacity exceedance (BC3)
$V_{c11}$	Crushing capacity of concrete strut (SC)

### 3.2. Failure Modes

Each failure mode is attained when the stress related to the involved element reaches its capacity. The weaker mechanism governs the structural capacity of the RC-joint, and three failure modes can be considered:

- A first failure mode is due to the conventional ultimate condition of reinforcement bars in tension: the yielding of longitudinal ( $V_{c5}$ ) or vertical reinforcement bars ( $V_{c7}$ );

- The debonding of longitudinal reinforcements associated with  $V_{c8}$ ,  $V_{c9}$ , and  $V_{c10}$ , related to maximum, average, and minimum bond capacity;
- Failure of concrete strut associated to column shear value  $V_{c11}$ .

The breakage or yielding of steel bars can be considered to be an ultimate condition for the cracked joint. In a cross-section with different number of bars,  $n_j$ , each with cross-section area,  $A_{k,i}$ , and characteristic ultimate stress due to yielding or ultimate stress,  $f_{yk}$ , the axial strength of longitudinal reinforcement can be easily calculated as:

$$F_{max,j} = \sum_{i=1}^{n_j} A_{k,i} \cdot f_{yk} \tag{16}$$

The maximum value,  $F_{max,j}$ , is related to the vertical or horizontal reinforcement layer. When this maximum value is reached in one of the reinforcement layers, the associated column shear,  $V_c$ , corresponds to the ultimate value,  $V_{c5}$ , for horizontal bars, and  $V_{c6}$  and  $V_{c7}$  involve the vertical steel bars of the top or bottom columns, respectively. The different values for top and bottom columns are due to the different axial load acting on the columns.

The failure mode, due to the de-bonding mechanism, is affected by a strong sensibility to the characteristics of steel bars. Different capacity models can be considered according to the existing literature. For this study, the model proposed in the model Code 2010 [86] has been chosen. It considered three values ( $\tau_{min}$ ,  $\tau_{av}$ ,  $\tau_{max}$ ) of the bond strength,  $\tau$ , as a function of the compressive strength of concrete,  $f_c$ , both expressed in MPa in dimensional Equations (17)–(19), and the characteristics of steel bars. In such equations, the numerical coefficients,  $k_{min}$ ,  $k_{av}$ , and  $k_{max}$ , are in  $MPa^{1/2}$ . The minimum value is related to the smooth bars, typical of existing RC buildings built before the 1960s.

$$\tau_{min} = k_{min} \sqrt{f_c} = 0.3 \sqrt{f_c} \tag{17}$$

$$\tau_{av} = k_{av} \sqrt{f_c} = 1.25 \sqrt{f_c} \tag{18}$$

$$\tau_{max} = k_{max} \sqrt{f_c} = 2.5 \sqrt{f_c} \tag{19}$$

After cracking, the RC joint is ideally discretized by means of four rigid portions. The maximum bond force is given by the lateral surface of bars multiplied by the strength,  $\tau$ . Diagonal cracks cut the joint in rigid portions, providing the length,  $L_{eb}$ , where bond strength contribution develops (Equation (20)). For the T-shaped RC joint, the bond force changes with the shear (positive or negative direction) and with the location of bars (upper and bottom layer).

Once the effective length,  $L_{eb}$ , is estimated, the bond capacity of concrete can be compared to the bond demand. The bond capacity is estimated assuming a uniform bond stress,  $\tau$ . For T-shaped RC joints under negative shear, the bond force is  $F1 + S4$  in the upper layer of bars, while it becomes  $F7 + S6$ , at the bottom side. When the shear becomes negative, the bond force is  $F4 + S1$  and  $F6 + S7$ , respectively, at the upper and lower side. For X-shaped RC joints, only the Equation (24) must be considered, due to the symmetry. For this reason, it is important to split the resultant compressive force into two contributions, due to the steel,  $S_i$ , and concrete,  $C_i$ . Figure 2a,b show the contribution due to the internal force under positive column shear (Figure 1b). Under a generic column shear (T or X-shaped RC joint), there are four steel contributions that can be calculated, for instance, starting from the following elastic equilibrium Equations (21)–(24). The neutral axis,  $y$ , can be evaluated, for instance, in pure flexure, equating the first order moment to zero [77].

$$L_{eb} = \frac{h_b^*}{\tan\theta} \tag{20}$$

$$\left( S4 - F7 \frac{A_s'(2y - H_b + h_b^*)}{A_s(H_b - h_b^* - 2y)} \right) i = 0 \tag{21}$$

$$\left( S6 - F_1 \frac{A_s(2y - H_b + h_b^*)}{A'_s(H_b + h_b^* - 2y)} \right) i = 0 \quad (22)$$

$$\left( S7 - F_4 \frac{A_s(2y - H_b + h_b^*)}{A'_s(H_b + h_b^* - 2y)} \right) i = 0 \quad (23)$$

$$S1 - \left( F_6 \frac{A_s}{A'_s} i + F_4 \frac{A'_s}{A_s} (1 - i) \right) \frac{(2y - H_b + h_b^*)}{(H_b + h_b^* - 2y)} = 0 \quad (24)$$

In previous equations, the cross-section of reinforcement in compression,  $A'_s$ , and tension,  $A_s$ , is introduced.

The column shear,  $V_c$ , due to the maximum bond force, provides the ultimate column shears,  $V_{c8}$  to  $V_{c10}$ . This value depends on the bond quality conditions.

The crushing of concrete strut yields to another failure mode. The maximum column shear,  $V_{c11}$ , is related to this failure mode. The maximum value of the compressed concrete force,  $C$ , (please note that it is different from  $C_i$ ) is governed by the compression strength (of concrete),  $f_c$ :

$$C_{max} = B \cdot f_c \frac{H_b}{2 \cdot \sin \vartheta} \quad (25)$$

$\vartheta$  is the inclination angle of the compressed concrete force,  $C$  (Figure 3). This value is potentially different from the diagonal crack angle  $\theta$  (Figure 3). Concrete contact force,  $C$ , inclination can be assumed to be different from the diagonal crack (i.e.,  $\vartheta \neq \theta$ ) if shear friction is assumed along cracks. Hence, shear friction, measured as deviation from diagonal (i.e.,  $|\vartheta - \theta|$ ), should be limited to a threshold capacity value. Compressed strength achievement yields to the corresponding column shear ultimate value of  $V_{c11}$ .

The previously discussed failure modes are related to the RC joint only. However, a check on the flexural capacity of both beam,  $M_b$ , and column,  $M_c$ , is necessary. It can be easily performed by using the classical capacity model of RC cross-sections. The top and bottom columns present different flexural capacities due to different axial loads. The maximum column shear related to the collapse of beam or columns can be easily expressed with Equations (11)–(14).

### 3.3. Experimental Validation

Experimental tests performed on real T- and X-shaped RC joints have been used to validate the proposed analytical model. Parate and Kumar [79] have compiled a database with 492 experimental results of beam-column joints from the literature. This database was used to validate the proposed analytical model. The full database is related to several types of RC joints. In particular, 270 specimens refer to T-shaped RC joints, while 222 specimens refer to X-shaped RC joints.

The T-shaped joints were analyzed under positive and negative column shear,  $V_c$ . The several experimental programs provide the basic information for applying the proposed model. Unfortunately, not all information is available from the literature. In particular, for some specimens, the bond characteristic of the reinforcement bars was not disclosed. For this reason, the three levels of maximum bond stress, according to Equations (17)–(19), have been considered. Therefore, the impact of the bond stress on the ultimate capacity of the RC-joint has been assessed. This approach has been performed on the entire population.

All information about the entire population has not been thoroughly discussed in this paper, due to the large number of specimens. For additional information, the reader could refer to the specific reference [79]. However, it is interesting to observe the main characteristics of the population. The main geometrical characteristics (depth and height) of the frame elements (beams and columns) are shown in Figure 4a,b for T- and X-shaped RC joints, respectively. The geometrical characteristics of the population embrace an ample range of typical values found in the existing building stock. Figure 5a,b show the amount of the longitudinal bars in the frame elements for the T- and X-shaped RC joints, respectively. The amount of reinforcement cross-section areas can be considered representative both of

existing and new RC buildings. Finally, the mechanical characteristics of concrete are shown in Figure 6a,b for T- and X-shaped RC joints. The mechanical performance of concrete can be considered typically representative of existing and new RC buildings. Therefore, this large sample size provides a good database for validating the proposed analytical model; however, some specimens of the dataset are not usual, both in terms of geometrical and mechanical characteristics.

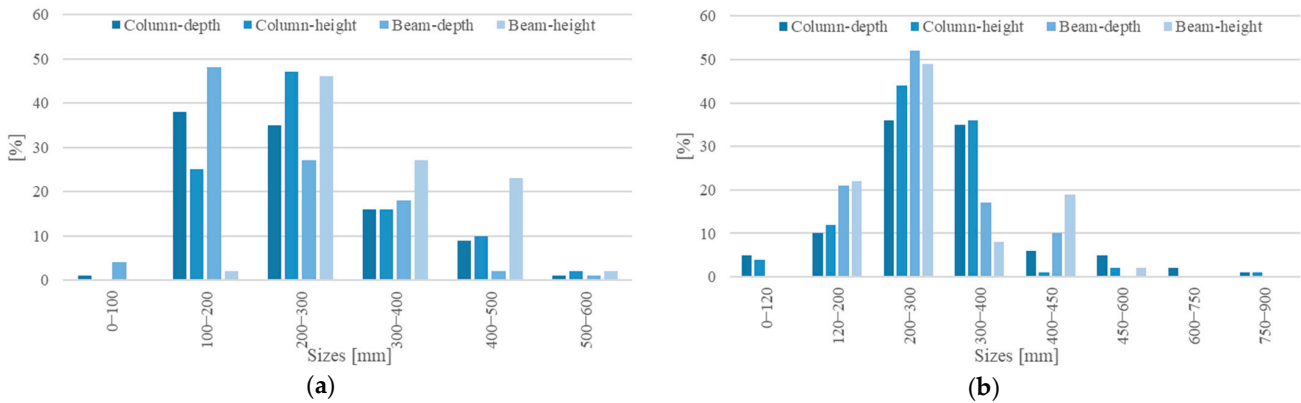


Figure 4. Geometrical characteristics of RC frame elements (column and beams): (a) T-shaped RC joints, (b) X-shaped RC joints.

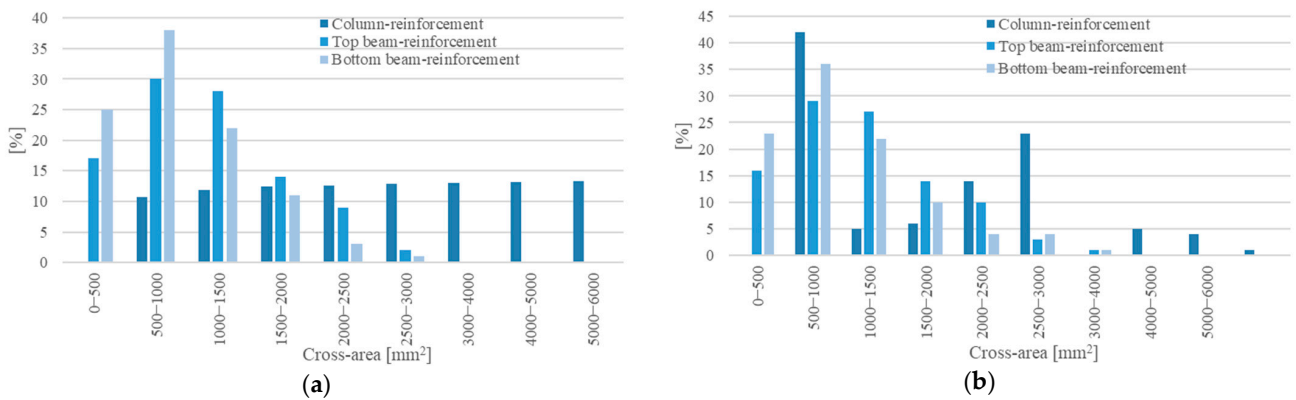


Figure 5. Geometrical characteristics of longitudinal reinforcements of RC frame elements (column and beams): (a) T-shaped RC joints, (b) X-shaped RC joints.

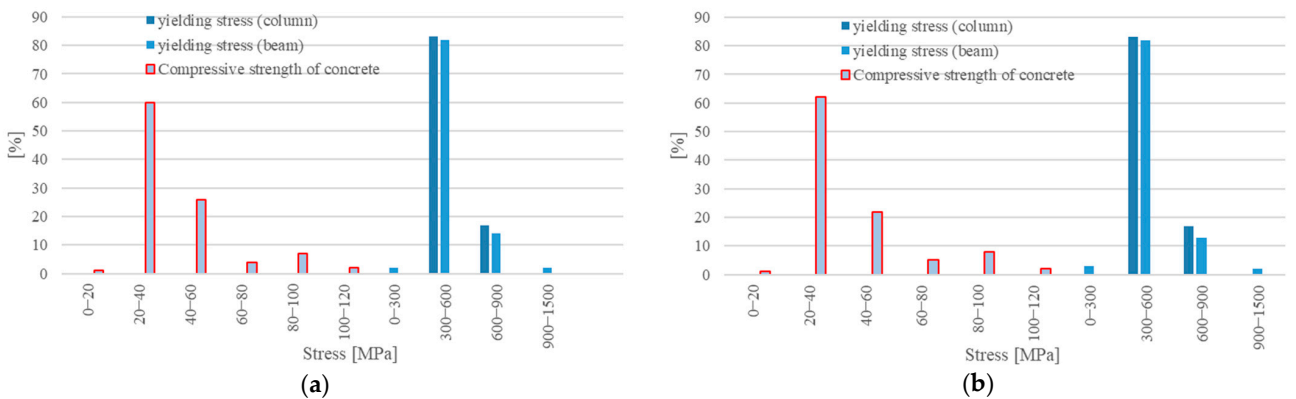
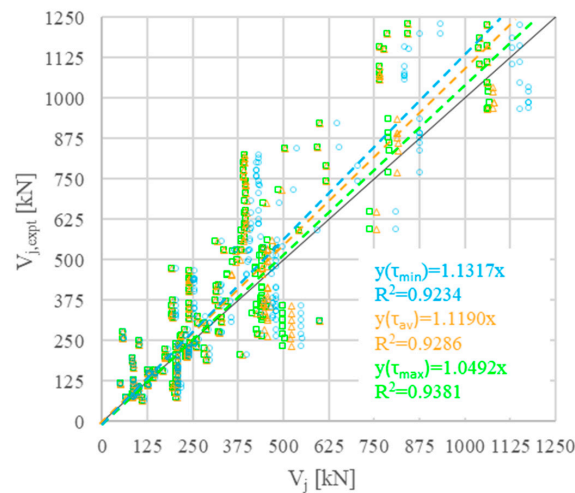


Figure 6. Mechanical performance of material of RC frame elements (column and beams): (a) T-shaped RC joints, (b) X-shaped RC joints.

The proposed model allows us to check the failure mode which occurred for the RC-joint. Unfortunately, this information is not available for some experimental tests.

Therefore, the comparison between the failure mode which was experimentally detected and the one which was numerically predicted has not been performed. The analytical results are shown by fixing the three values of bond stress according to Equations (17)–(19). The same bond stress yields to different bond capacities at different layers of bars (top and bottom) if different bars are present. Since, in X-shaped RC joints, the demands at the top and bottom layers of bars are equal, the bond capacity yielding to the failure is provided by the minimum amount of steel bars at the bottom or top layers. Conversely, for T-shaped RC joints, the bond demand depends on the sign of column shear; hence, the check should be performed both at the bottom and top layers of bars, because the bond capacity could also change at the two layers. Figure 7 shows the comparison between the experimental results and the analytical predictions related to the T-shaped joints under positive column shear. The figure shows the analytical and experimental value of column shear,  $V_j$  and  $V_{j,exp}$ , respectively. The diagonal black line represents the ideal condition where the experimental value coincides with the analytical prevision (line with unitary slope); the red represents the best interpolating line of the points crossing the origin. Furthermore, the coefficient of determination,  $R^2$ , is shown for each case. The same analysis was performed for T-shaped RC joints under negative column shear (Figure 8) and the X-shaped RC joints (Figure 9).



**Figure 7.** Experimental and numerical comparison for T-shaped RC joints under positive column shear: minimum bond stress (blue), average bond stress (orange), and maximum bond stress (green).

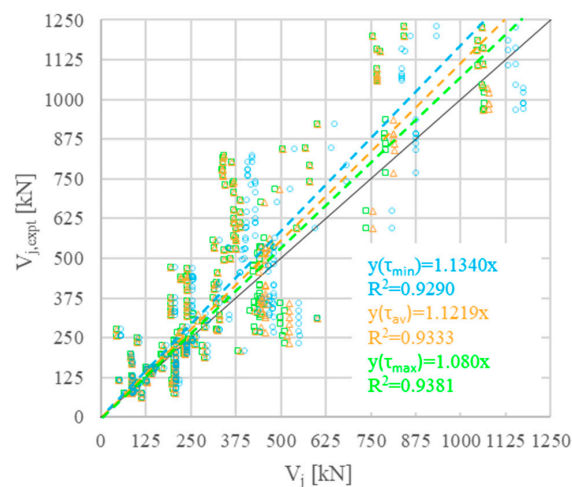


**Figure 8.** Experimental and numerical comparison for T-shaped RC joints under negative column shear: minimum bond stress (blue), average bond stress (orange), and maximum bond stress (green).

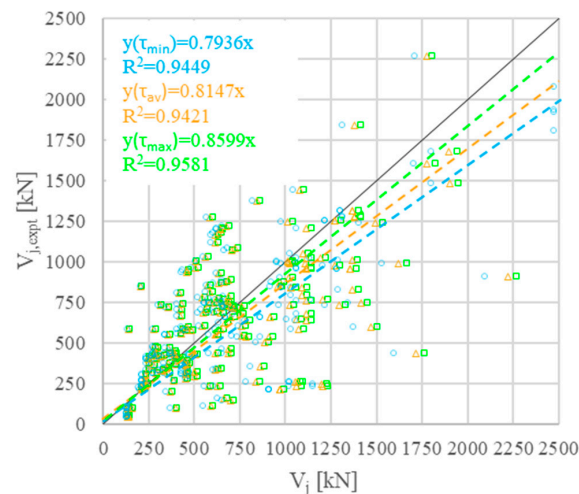


**Figure 9.** Experimental and numerical comparison for X-shaped RC joints: minimum bond stress (blue), average bond stress (orange), and maximum bond stress (green).

The previous figures show the impact of the bond stress (minimum, average, and maximum value) on the ultimate capacity of RC-joints. It is worth noting that the analytical predictions slightly worsen when the bond stress decreases. However, this effect appears to be negligible in the entire population. Under positive or negative column shear, the coefficient of determination undergoes very small variations for T-shaped RC joints. Only for negative column shear does the coefficient of determination decrease, moving from the minimum to average bond stress, while it weakly increases when the maximum bond stress is considered. This effect is likely due to the characteristics of the experimentally tested specimens. Furthermore, the characteristics of the bond condition strongly depend on the construction of the RC joints. For this reason, the comparison was performed while changing parametrically the characteristics of bond conditions. Under both positive and negative column shear, the analytical predictions fit well with the experimental results. It is confirmed by the coefficient of determination,  $R^2$ , and slope of the interpolating line, which are both very close to 1.

The same analysis was performed for X-shaped RC joints. The comparison between the experimental and the analytical predictions show a higher dispersion compared to the case of T-shaped RC joints. However, given the large number of specimens, it was noted that some specimens exhibited non-typical behavior. In fact, in analyzing some experimental results, it is clear that some values are not typical for the materials. These differences are apparently due to particular test conditions. A screening of some test values could be useful to eliminate unrealistic results; however, the authors preferred to consider the entire population instead of filtering data, since not all of the information is available. The dispersion changes slightly with the considered bond capacities; thus, the ultimate behavior of X-shaped joints appears to be weakly influenced by the bond capacity of the reinforcement layer.

The proposed model allows the assessment of the failure mode to be linked to the ultimate capacity of RC joints. It is worth noting that the failure mode varies as some input parameters change. According to the experimental database, the impact of the bond stress on the ultimate capacity was noted. In particular, the bond stress has been changed according to the Equations (17)–(19) for the entire sample, and the related failure mode was assessed. Figure 10a,b refer to the T-shaped joints under positive and negative column shear, respectively, while Figure 10c shows the same result for X-shaped joints.

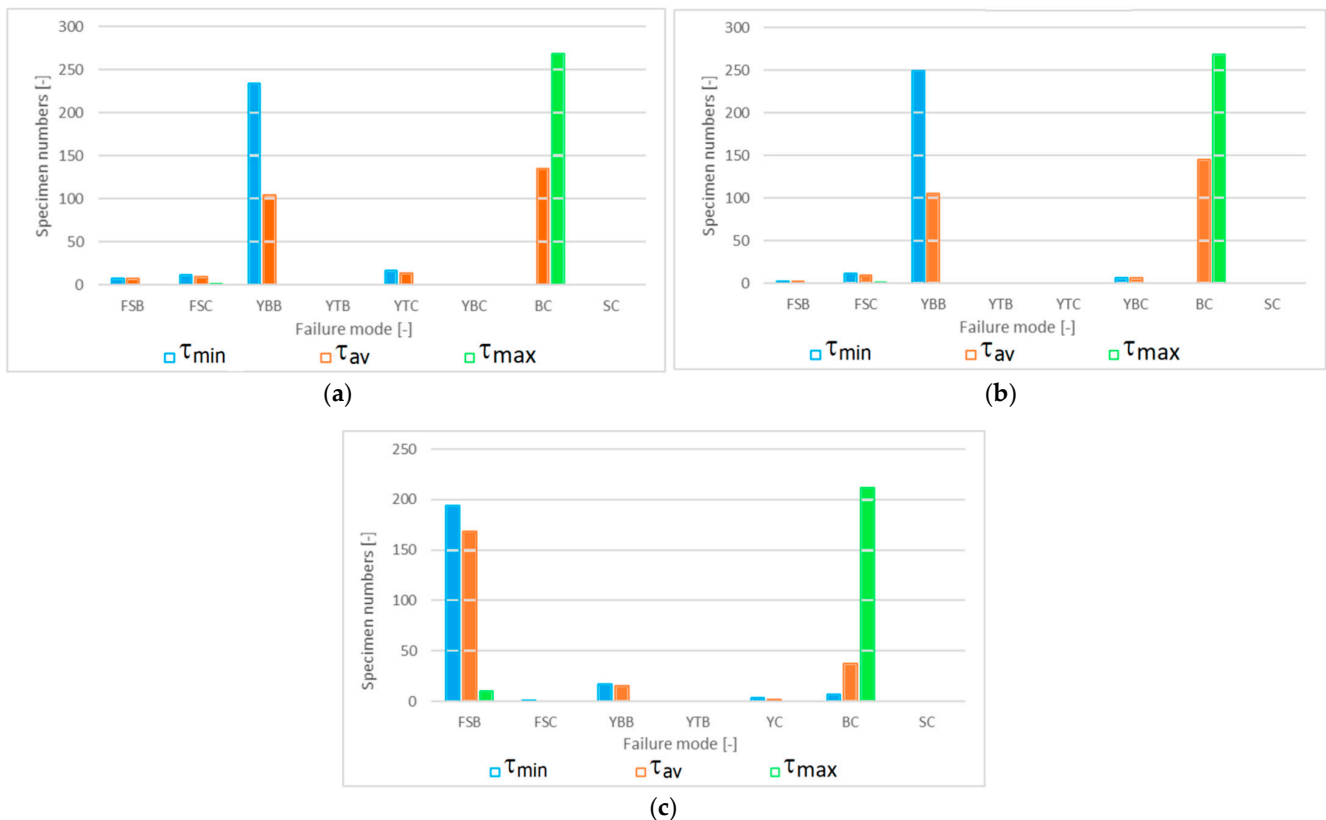


**Figure 10.** Failure mode as the bond stress changes: (a) T-shaped RC joints under positive column shear, (b) T-shaped RC joints under negative column shear, and (c) X-shaped RC joints.

It is worth noting that the sign of column shear strongly influences the failure mode of T-shaped RC joints. Decreasing the bond stress value, the failure mode is due to the bond capacity exceedance for almost the entire population. Under a negative column shear, a non-negligible number of specimens showed a yielding failure mode of vertical bars in the bottom column, despite a minimum bond stress having been considered. Furthermore, decreasing the bond stress for T-shaped RC joints, the failure mode becomes influenced by the layer of reinforcement bars where the yielding occurred. For a maximum (19) and average (18) value of the bond capacity, the yielding of horizontal bars appears to be a recurrent failure mode for the entire population (T-shaped RC joints). The X-shaped joints showed a different failure mode when the maximum bond capacity was assumed. In particular, almost the entire population showed an ultimate capacity due to the flexural capacity of beams, while the percentage of specimens that showed the yielding of longitudinal or vertical bars remains low. These alterations are due to the different geometry of frame elements related to T- and X-shaped joints, as well as the effect of axial load on lower columns.

The analytical predictions provided by the proposed model for X-shaped RC joints are less reliable than that for T-shaped ones. However, it is interesting to compare the proposed model with the main building code predictions. Parate and Kumar, in 2019 [79], compared code predictions (average values) with experimental results. The comparison was performed in terms of predicted ultimate column shear,  $V_j$  ratio, with the experimental results,  $V_{j\text{expt}}$ . Tables 2 and 3 show the comparison of the ratios of different building codes [12,87–91] and of proposed model predictions with the experimental results for both T- and X-shaped RC joints, respectively, in terms of average value,  $\mu$ , standard deviation,  $\sigma$ , and coefficient of variation (CV). The statistical results for the proposed model refer to the three bond conditions, according to Equations (17)–(19).

**Table 2.** Average value,  $\mu$ , standard deviation,  $\sigma$ , and coefficient of variation (CV) of the ratios of experimental ultimate column shear and available prediction models for T-shaped RC joints.

Type	Prediction Models												
	T-Shaped	ACI 318-14	EN1998-1:2004	NZS 3101:1-2006	CSA A23.3:2004	AIJ: 2010	IS 13920: 2016	Proposed Model, $V_j > 0$			Proposed Model, $V_j < 0$		
								$\tau_{\min}$	$\tau_{\text{av}}$	$\tau_{\max}$	$\tau_{\min}$	$\tau_{\text{av}}$	$\tau_{\max}$
$\mu$	0.95	0.92	0.73	1.08	1.33	1.15	0.98	0.98	0.96	0.98	0.98	0.96	
$\sigma$	0.38	0.56	0.32	0.40	0.47	0.4	0.07	0.07	0.09	0.08	0.08	0.07	
CV	0.4	0.61	0.46	0.37	0.35	0.35	0.07	0.07	0.8	0.08	0.08	0.07	

**Table 3.** Average value,  $\mu$ , standard deviation,  $\sigma$ , and coefficient of variation (CV) of the ratios of experimental ultimate column shear and available prediction models for X-shaped RC joints.

Type	Prediction Models									
	X-Shaped	ACI 318-14	EN1998-1:2004	NZS 3101:1-2006	CSA A23.3:2004	AIJ: 2010	IS 13920: 2016	Proposed Model		
								$\tau_{\min}$	$\tau_{\text{av}}$	$\tau_{\max}$
$\mu$	0.89	0.76	0.89	1.02	0.71	1.11	1.03	1.02	1.04	
$\sigma$	0.45	0.44	0.50	0.52	0.33	0.56	0.07	0.09	0.08	
CV	0.50	0.58	0.56	0.5	0.47	0.5	0.08	0.09	0.09	

The comparison between experimental results and predictions in terms of statistical parameters provides valuable information on the reliability of the available models. Significant dispersion is found for code predictions, while the proposed model best fits the experimental results for T-shaped RC joints. Furthermore, the results are always conservative, with respect to the experimental ones. For the X-shaped RC joints, a greater dispersion was found, and the results appear to be, on average, non-conservative. However, it is interesting to observe how the coefficient of variation is lower compared to that provided by the other available models [12,87–91].

#### 4. Conclusions

The present study proposes a unified analytical model to assess the ultimate capacity of RC beam-column joints. The model was developed according to a generalized approach. It allows the behavior of both T- and X-shaped RC joints to be assessed by means of a single mathematical model.

The proposed approach allows for the evaluation of several failure modes typically detected in the RC joints. It represents an important improvement, especially in practical applications.

The present study contributed a theoretical discussion of the failure mechanisms of RC joints. The failure modes can be different, and to have a model able to assess them represents a valid tool, especially for the designers. In particular, predictions can be used to check the most satisfactory mechanism compared to the others. Therefore, the proposed simplified model is useful for this purpose, due to the possibility of checking these differences.

These predictions represent the basis for the effort to drive the design towards the respect of the strength hierarchy. The advantages of a ductile failure mode in the case of a seismic event are known and largely debated by the scientific community, preserving the joints from premature failures.

The comparison between the analytical predictions and approximately 500 experimental results confirmed the reliability of the proposed model. The proposed model is able to indicate the failure mode, as well, for each specimen of the large experimental population.

The impact of the bond condition has been evaluated on several types of RC joints (T- and X-shaped), highlighting the differences between these two shapes. These outcomes provide a useful contribution to understanding which mechanism, as the input parameters change, led to ultimate capacity of the RC joints and their relation.

**Author Contributions:** Conceptualization, G.P.L.; methodology, G.P.L.; software, G.P.L.; investigation, G.R., G.P.L. and F.F.; data curation, G.R.; writing—original draft preparation, G.R. and G.P.L.; writing—review and editing, F.F. and A.P.; supervision, A.P. All authors have read and agreed to the published version of the manuscript.

**Funding:** This research received no external funding.

**Data Availability Statement:** The data that support the findings of this study are available upon reasonable request.

**Conflicts of Interest:** The authors have no conflict of interest to declare.

## References

1. IBC. Italian Building Code: Ministerial Decree 17 January 2018. In *Aggiornamento Delle Norme Tecniche delle Costruzioni*; Ministry of Infrastructure and Transport: Rome, Italy, 2018.
2. *EN 1992-1:2004 Eurocode 2*; Design of Concrete Structures, Part 1-1: General Rules, Seismic Actions and Rules for Buildings. European Committee for Standardization (CEN): Brussels, Belgium, 2014.
3. Lakusic, S. Seismic vulnerability of an existing strategic RC building using non linear static and dynamic analyses. *J. Croat. Assoc. Civ. Eng.* **2020**, *72*, 617–626. [[CrossRef](#)]
4. Dilmaç, H. Preliminary assessment approach to predict seismic vulnerability of existing low and mid-rise RC buildings. *Bull. Earthq. Eng.* **2020**, *18*, 3101–3133. [[CrossRef](#)]
5. Caprili, S.; Nardini, L.; Salvatore, W. Evaluation of seismic vulnerability of a complex RC existing building by linear and nonlinear modeling approaches. *Bull. Earthq. Eng.* **2012**, *10*, 913–954. [[CrossRef](#)]
6. Shayanfar, J.; Bengar, H.A.; Parvin, A. Analytical prediction of seismic behavior of RC joints and columns under varying axial load. *Eng. Struct.* **2018**, *174*, 792–813. [[CrossRef](#)]
7. Jung, W.; Kim, J.; Kwon, M. Performance evaluation of RC beam-column joints with different bonding interfaces. *Sci. Iran.* **2018**, *25*, 11–21. [[CrossRef](#)]
8. Yang, Y.; Xue, Y.; Wang, N.; Yu, Y. Experimental and numerical study on seismic performance of deficient interior RC joints retrofitted with prestressed high-strength steel strips. *Eng. Struct.* **2019**, *190*, 306–318. [[CrossRef](#)]
9. Li, Z.; Liu, Y.; Huo, J.; Elghazouli, A.Y. Experimental and analytical assessment of RC joints with varying reinforcement detailing under push-down loading before and after fires. *Eng. Struct.* **2019**, *189*, 550–564. [[CrossRef](#)]
10. Vargas, Y.F.; Pujades, L.G.; Barbat, A.H.; Hurtado, J.E. Probabilistic Seismic Damage Assessment of RC Buildings Based on Nonlinear Dynamic Analysis. *Open Civ. Eng. J.* **2018**, *9*, 344–350. [[CrossRef](#)]
11. Pepe, V.; De Angelis, A.; Pecce, M.R. Damage assessment of an existing RC infilled structure by numerical simulation of the dynamic response. *J. Civ. Struct. Health Monit.* **2019**, *9*, 385–395. [[CrossRef](#)]
12. *EN 1998-1:2004: Eurocode 8*; Design of Structures for Earthquake Resistance—Part 1: General Rules, Seismic Actions and Rules for Buildings. Authority: The European Union per Regulation 305/2011, Directive 98/34/EC, Directive 2004/18/EC. European Committee for Standardization (CEN): Brussels, Belgium, 2004.
13. Abdelwahed, B. A review on building progressive collapse, survey and discussion. *Case Stud. Constr. Mater.* **2019**, *11*, e00264. [[CrossRef](#)]
14. Pachla, F.; Kowalska-Koczwara, A.; Tatara, T.; Stypuła, K. The influence of vibration duration on the structure of irregular RC buildings. *Bull. Earthq. Eng.* **2019**, *17*, 3119–3138. [[CrossRef](#)]
15. Tasligedik, A.S.; Akguzel, U.; Kam, W.Y.; Pampanin, S. Strength Hierarchy at Reinforced Concrete Beam-Column Joints and Global Capacity. *J. Earthq. Eng.* **2018**, *22*, 454–487. [[CrossRef](#)]
16. Sangiorgio, V.; Uva, G.; Aiello, M.A. A multi-criteria-based procedure for the robust definition of algorithms aimed at fast seismic risk assessment of existing RC buildings. *Structures* **2020**, *24*, 766–782. [[CrossRef](#)]
17. Tasligedik, A.S. Shear Capacity N-M Interaction Envelope for RC Beam-Column Joints with Transverse Reinforcement: A Concept Derived from Strength Hierarchy. *J. Earthq. Eng.* **2022**, *26*, 2194–2224. [[CrossRef](#)]
18. Pantelides, C.P.; Hansen, J.; Ameli, M.J.; Reaveley, L.D. Seismic performance of reinforced concrete building exterior joints with substandard details. *J. Struct. Integr. Maint.* **2017**, *2*, 1–11. [[CrossRef](#)]
19. Ma, G.; Li, H.; Hwang, H.J. Seismic behavior of low-corroded reinforced concrete short columns in an over 20-year building structure. *Soil Dyn. Earthq. Eng.* **2018**, *106*, 90–100. [[CrossRef](#)]
20. De Risi, M.T.; Verderame, G.M. Experimental assessment and numerical modelling of exterior non-conforming beam-column joints with plain bars. *Eng. Struct.* **2017**, *150*, 115–134. [[CrossRef](#)]
21. Do, V.T.; Pham, V.V.; Nguyen, H.N. On the development of refined plate theory for static bending behaviour of functionally graded plates. *Math. Probl. Eng.* **2020**, *2020*, 2836763. [[CrossRef](#)]
22. Hoa, L.K.; Pham, V.V.; Dinh Duc, N.; Thoi Trung, N.; Truong Son, L.; Thom, D.V. Bending and free vibration analyses of functionally graded material nanoplates via a novel nonlocal single variable shear deformation plate theory. *J. Mech. Eng. Sci.* **2020**, *235*, 3641–3653. [[CrossRef](#)]

23. Tran, T.T.; Nguyen, H.N.; Do, V.T.; Minh, P.V.; Dinh Duc, N. Bending and thermal buckling of unsymmetric functionally graded sandwich beams in high-temperature environment based on a new third-order shear deformation theory. *J. Sandw. Struct. Mater.* **2019**, *23*, 906–930. [[CrossRef](#)]
24. Duc, N.D.; Trinh, T.D.; Do, T.V.; Doan, D.H. On the buckling behavior of multi-cracked FGM plates. In Proceedings of the International Conference on Advances in Computational Mechanics (ACOME 2017), Phu Quoc, Vietnam, 2–4 August 2017. [[CrossRef](#)]
25. Pauletta, M.; Di Marco, C.; Frappa, G.; Somma, G.; Iginio, P.; Miani, M.; Da, S.; Russo, G. Semi-empirical model for shear strength of RC interior beam-column joints subjected to cyclic loads. *Eng. Struct.* **2020**, *224*, 111223. [[CrossRef](#)]
26. Pauletta, M.; Di Marco, C.; Frappa, G.; Miani, M.; Campione, G.; Russo, G. Seismic behavior of exterior RC beam-column joints without code-specified ties in the joint core. *Eng. Struct.* **2020**, *228*, 111542. [[CrossRef](#)]
27. Shafaei, J.; Hosseini, A.; Marefat, M.S.; Ingham, J.M.; Zare, H. Experimental Evaluation of Seismically and Non-Seismically Detailed External RC Beam-Column Joints. *J. Earthq. Eng.* **2017**, *21*, 776–807. [[CrossRef](#)]
28. Pantelides, C.P.; Hansen, J.; Nadauld, J.; Reaveley, L.D. *Assessment of Reinforced Concrete Building Exterior Joints with Substandard Details*; Technical Report No. 2002/18 PEER; Pacific Earthquake Engineering Research Center: Berkeley, CA, USA, 18 May 2002.
29. Yurdakul, Ö.; Del Vecchio, C.; Di Ludovico, M.; Avşar, Ö. Numerical simulation of substandard beam-column joints with different failure mechanisms. *Struct. Concr.* **2020**, *21*, 2515–2532. [[CrossRef](#)]
30. Lu, Y.; Tang, W.; Li, S.; Tang, M. Effects of simultaneous fatigue loading and corrosion on the behavior of reinforced beams. *Constr. Build. Mater.* **2018**, *181*, 85–93. [[CrossRef](#)]
31. Shayanfar, J.; Hemmati, A.; Bengar, H.A. A simplified numerical model to simulate RC beam-column joints collapse. *Bull. Earthq. Eng.* **2019**, *17*, 803–844. [[CrossRef](#)]
32. Xie, L.; Lu, X.; Guan, H.; Lu, X. Experimental Study and Numerical Model Calibration for Earthquake-Induced Collapse of RC Frames with Emphasis on Key Columns, Joints, and the Overall Structure. *J. Earthq. Eng.* **2015**, *19*, 1320–1344. [[CrossRef](#)]
33. Shafaei, J. Non-linear macro modelling of cyclic response of non-seismically detailed reinforced-concrete connections. *Mag. Concr. Res.* **2021**, *73*, 80–97. [[CrossRef](#)]
34. Rizwan, M.; Ahmad, N.; Naeem Khan, A.; Qazi, S.; Akbar, J.; Fahad, M. Shake table investigations on code non-compliant reinforced concrete frames. *Alex. Eng. J.* **2020**, *59*, 349–367. [[CrossRef](#)]
35. Cheng, J.; Luo, X.; Xiang, P. Experimental study on seismic behavior of RC beams with corroded stirrups at joints under cyclic loading. *J. Build. Eng.* **2020**, *32*, 101489. [[CrossRef](#)]
36. Jin, L.; Miao, L.; Han, J.; Du, X.; Wei, N.; Li, D. Size effect tests on shear failure of interior RC beam-to-column joints under monotonic and cyclic loadings. *Eng. Struct.* **2018**, *175*, 591–604. [[CrossRef](#)]
37. Wang, N.; Shi, Q.X. Shear model and nonlinear analysis of rc beam-column joint with high-strength stirrups. *Gongcheng Lixue/Eng. Mech.* **2017**, *34*, 89–96. [[CrossRef](#)]
38. Moodi, Y.; Sohrabi, M.R.; Mousavi, S.R. Effects of stirrups in spliced region on the bond strength of corroded splices in reinforced concrete (RC) beams. *Constr. Build. Mater.* **2020**, *230*, 116873. [[CrossRef](#)]
39. Jin, L.; Du, M.; Li, D.; Du, X.; Xu, H. Effects of cross section size and transverse rebar on the behavior of short squared RC columns under axial compression. *Eng. Struct.* **2017**, *142*, 223–239. [[CrossRef](#)]
40. Aly, N.; AlHamaydeh, M.; Galal, K. Quantification of the Impact of Detailing on the Performance and Cost of RC Shear Wall Buildings in Regions with High Uncertainty in Seismicity Hazards. *J. Earthq. Eng.* **2018**, *24*, 421–446. [[CrossRef](#)]
41. Chiu, C.K.; Noguchi, T.; Kanematsu, M. Effects of maintenance strategies on the life-cycle performance and cost of a deteriorating RC building with high-seismic hazard. *J. Adv. Concr. Technol.* **2010**, *8*, 157–170. [[CrossRef](#)]
42. Cardone, D.; Gesualdi, G.; Perrone, G. Cost-Benefit Analysis of Alternative Retrofit Strategies for RC Frame Buildings. *J. Earthq. Eng.* **2019**, *23*, 208–241. [[CrossRef](#)]
43. O'Reilly, G.J.; Sullivan, T.J. Probabilistic seismic assessment and retrofit considerations for Italian RC frame buildings. *Bull. Earthq. Eng.* **2018**, *16*, 1447–1485. [[CrossRef](#)]
44. Di Lorenzo, G.; Colacurcio, E.; Di Filippo, A.; Formisano, A.; Massimilla, A.; Landolfo, R. State-of-the-art on steel exoskeletons for seismic retrofit of existing RC buildings. *Ing. Sismica* **2020**, *37*, 33–49.
45. Al-Sherrawi, M.H.; Salman, H.M. Analytical Model for Construction of Interaction Diagram for RC Columns Strengthened by Steel Jacket. *Int. J. Sci. Res.* **2015**, *6*, 324–328. [[CrossRef](#)]
46. He, A.; Cai, J.; Chen, Q.J.; Liu, X.; Xu, J. Behaviour of steel-jacket retrofitted RC columns with preload effects. *Thin-Walled Struct.* **2016**, *109*, 25–39. [[CrossRef](#)]
47. Nechevska-Cvetanovska, G.; Rosh, A. Rehabilitation of RC buildings in seismically active regions using traditional and innovative materials. *Gradjevinski Mater. I Konstr.* **2019**, *62*, 19–30. [[CrossRef](#)]
48. Imjai, T.; Setkit, M.; Garcia, R.; Sukontasukkul, P.; Limkatanyu, S. Seismic strengthening of low strength concrete columns using high ductile metal strap confinement: A case study of kindergarten school in Northern Thailand. *Walailak J. Sci. Technol.* **2020**, *17*, 1335–1347. [[CrossRef](#)]
49. Bournas, D.A. Concurrent seismic and energy retrofitting of RC and masonry building envelopes using inorganic textile-based composites combined with insulation materials: A new concept. *Compos. Part B Eng.* **2018**, *148*, 166–179. [[CrossRef](#)]
50. Jagtap, A.D.; Dhawade, S.M. Benefits of Prefabricated Building Material Over on Site Construction-A Review. *International Journal of Research in Engineering, Science and Technologies (IJRESTS). Civ. Eng.* **2015**, *1*, 195–202.

51. Bianchi, F.; Nascimbene, R.; Pavese, A. Experimental vs. Numerical Simulations: Seismic Response of a Half Scale Three-Storey Infilled RC Building Strengthened Using FRP Retrofit. *Open Civ. Eng. J.* **2018**, *11*, 1158–1169. [[CrossRef](#)]
52. Dang, C.T.; Dinh, N.H. Experimental Study on Structural Performance of RC Exterior Beam-Column Joints Retrofitted by Steel Jacketing and Haunch Element under Cyclic Loading Simulating Earthquake Excitation. *Adv. Civ. Eng.* **2017**, *2017*, 9263460. [[CrossRef](#)]
53. Zinno, A.; Lignola, G.P.; Prota, A.; Manfredi, G.; Cosenza, E. Influence of free edge stress concentration on effectiveness of FRP confinement. *Compos. Part B Eng.* **2010**, *41*, 523–532. [[CrossRef](#)]
54. Ilkhani, M.H.; Naderpour, H.; Kheyroddin, A. Soft computing-based approach for capacity prediction of FRP-strengthened RC joints. *Sci. Iran.* **2019**, *26*, 2678–2688. [[CrossRef](#)]
55. Niroomandi, A.; Maheri, A.; Maheri, M.R.; Mahini, S.S. Seismic performance of ordinary RC frames retrofitted at joints by FRP sheets. *Eng. Struct.* **2010**, *32*, 2326–2336. [[CrossRef](#)]
56. Giamundo, V.; Lignola, G.P.; Prota, A.; Manfredi, G. Analytical evaluation of FRP wrapping effectiveness in restraining reinforcement bar buckling. *Anal. Eval. FRP Wrap. Eff. Restraining Reinf. Bar Buckling* **2014**, *140*, 04014043. [[CrossRef](#)]
57. Yang, Z.; Liu, Y.; Li, J. Study of Seismic Behavior of RC Beam-Column Joints Strengthened by Sprayed FRP. *Adv. Mater. Sci. Eng.* **2018**, *2018*, 3581458. [[CrossRef](#)]
58. Faleschini, F.; Gonzalez-Libreros, J.; Zanini, M.A.; Hofer, L.; Sneed, L.; Pellegrino, C. Repair of severely-damaged RC exterior beam-column joints with FRP and FRCM composites. *Compos. Struct.* **2019**, *207*, 352–363. [[CrossRef](#)]
59. Al-Salloum, Y.A.; Siddiqui, N.A.; Elsanadedy, H.M.; Abadel, A.A.; Aqel, M.A. Textile-reinforced mortar versus FRP as strengthening material for seismically deficient RC beam-column joints. *J. Compos. Constr.* **2011**, *15*, 920–933. [[CrossRef](#)]
60. Shang, X.; Yu, J.; Li, L.; Lu, Z. Strengthening of RC Structures by Using Engineered Cementitious Composites: A Review. *Sustainability* **2019**, *11*, 3384. [[CrossRef](#)]
61. Calabrese, A.S.; D'Antino, T.; Colombi, P.; Carloni, C.; Poggi, C. Fatigue behavior of PBO FRCM composite applied to concrete substrate. *Materials* **2020**, *13*, 2368. [[CrossRef](#)] [[PubMed](#)]
62. Cabral-Fonseca, S.; Correia, J.R.; Custódio, J.; Silva, H.M.; Machado, A.M.; Sousa, J. Durability of FRP—Concrete bonded joints in structural rehabilitation: A review. *Int. J. Adhes. Adhes.* **2018**, *83*, 153–167. [[CrossRef](#)]
63. Harrington, C.C.; Liel, A.B. Evaluation of Seismic Performance of Reinforced Concrete Frame Buildings with Retrofitted Columns. *J. Struct. Eng.* **2020**, *146*, 04020237. [[CrossRef](#)]
64. Basereh, S.; Okumus, P.; Aaleti, S. Seismic Retrofit of Reinforced Concrete Shear Walls to Ensure Reparability. In Proceedings of the Structures Congress 2020, St. Louis, MO, USA, 5–8 April 2020. [[CrossRef](#)]
65. Vielma-Perez, J.C.; Porcu, M.C.; Fuentes, M.A.G. Non-linear analyses to assess the seismic performance of RC buildings retrofitted with FRP. *Rev. Int. Metodos Numer. Para Calc. Y Diseno Ing.* **2020**, *36*, 24. [[CrossRef](#)]
66. Tran, C.T.N.; Li, B. Analytical Model for Shear-critical Reinforced Concrete Interior Beam-column Joints. *J. Earthq. Eng.* **2020**, *24*, 1205–1221. [[CrossRef](#)]
67. Wong, H.F.; Kuang, J.S. Predicting shear strength of RC interior beam-column joints by modified rotating-angle softened-truss model. *Comput. Struct.* **2013**, *133*, 12–17. [[CrossRef](#)]
68. Najafgholipour, M.A.; Dehghan, S.M.; Dooshabi, A.; Niroomandi, A. Finite element analysis of reinforced concrete beam-column connections with governing joint shear failure mode. *Lat. Am. J. Solids Struct.* **2017**, *14*, 1200–1225. [[CrossRef](#)]
69. Caprili, S.; Chellini, G.; Mattei, F.; Romis, F.; Salvatore, W. Experimental Assessment of the Cyclic Behaviour of RC-DP Beam to Column Joints. *J. Earthq. Eng.* **2020**, *26*, 2301–2327. [[CrossRef](#)]
70. Kim, J.; LaFave, J.M. Key influence parameters for the joint shear behaviour of reinforced concrete (RC) beam-column connections. *Eng. Struct.* **2007**, *29*, 2523–2539. [[CrossRef](#)]
71. Santarsiero, G.; Masi, A. Key Mechanisms of the Seismic Behaviour of External RC Wide Beam-column Joints. *Open Constr. Build. Technol. J.* **2019**, *13*, 36–51. [[CrossRef](#)]
72. Lima, C.; Martinelli, E. A low-cycle fatigue approach to predicting shear strength degradation in RC joints subjected to seismic actions. *Bull. Earthq. Eng.* **2019**, *17*, 6061–6078. [[CrossRef](#)]
73. Azim, I.; Yang, J.; Javed, M.F.; Iqbal, M.F.; Mahmood, Z.; Wang, F.; Liu, Q.F. Prediction model for compressive arch action capacity of RC frame structures under column removal scenario using gene expression programming. *Structures* **2020**, *25*, 212–228. [[CrossRef](#)]
74. Abdissa, G. Finite Element Analysis of Reinforced Concrete Interior Beam Column Connection Subjected to Lateral Loading. *Am. J. Civ. Eng.* **2020**, *8*, 20. [[CrossRef](#)]
75. Supaviriyakit, T.; Pimanmas, A.; Warnitchai, P. Nonlinear finite element analysis of nonseismically detailed interior rc beam-column connection under reversed cyclic load. *Asean J. Sci. Technol. Dev.* **2007**, *24*, 369–386. [[CrossRef](#)]
76. Pantò, B.; Caddemi, S.; Calì, I.; Spacone, E. A 2D beam-column joint macro-element for the nonlinear analysis of RC frames. *Earthq. Eng. Struct. Dyn.* **2021**, *50*, 935–954. [[CrossRef](#)]
77. Bossio, A.; Fabbrocino, F.; Lignola, G.P.; Prota, A.; Manfredi, G. Simplified Model for Strengthening Design of Beam-Column Internal Joints in Reinforced Concrete Frames. *Polymers* **2015**, *7*, 1732–1754. [[CrossRef](#)]
78. Bossio, A.; Fabbrocino, F.; Lignola, G.P.; Prota, A.; Manfredi, G. Design Oriented Model for the Assessment of T-Shaped Beam-Column Joints in Reinforced Concrete Frames. *Buildings* **2017**, *7*, 118. [[CrossRef](#)]

79. Parate, K.; Kumar, R. Shear strength criteria for design of RC beam–column joints in building codes. *Bulletin of Earthquake Engineering* **2019**, *17*, 1407–1493. [[CrossRef](#)]
80. Basha, A.M.; Fayed, S. Behavior of RC Eccentric Corner Beam-Column Joint under Cyclic Loading: An Experimental Work. *Civ. Eng. J.* **2019**, *5*, 295. [[CrossRef](#)]
81. Bilotta, A.; Cosenza, E. Shear capacity model for reinforced concrete joints. *Eng. Struct.* **2022**, *266*, 114631. [[CrossRef](#)]
82. Shiohara, H. New Model for Shear Failure of RC Interior Beam-Column Connections. *J. Struct. Eng.* **2001**, *127*, 152–160. [[CrossRef](#)]
83. Di Ludovico, M.; Lignola, G.P.; Prota, A.; Cosenza, E. Nonlinear analysis of cross sections under axial load and biaxial bending. *ACI Struct. J.* **2010**, *107*, 390–399.
84. Lignola, G.P.; Prota, A.; Manfredi, G. Simplified modeling of rectangular concrete cross-sections confined by external FRP wrapping. *Polymers* **2014**, *6*, 1187–1206. [[CrossRef](#)]
85. Lignola, G.P.; Nardone, F.; Prota, A.; Manfredi, G. Analytical model for the effective strain in FRP-wrapped circular RC columns. *Compos. Part B Eng.* **2012**, *43*, 3208–3218. [[CrossRef](#)]
86. CEB-FIP. *Model Code for Concrete Structures 2010*; Comité Euro-International du Béton, Wilhelm Ernst & Sohn: Berlin, Germany, 2013.
87. ACI Committee. *Building Code Requirements for Structural Concrete (ACI 318-14) and Commentary (ACI 318R-14)*; American Concrete Institute: Farmington Hills, MI, USA, 2014.
88. *NZS 3101.1:2006*; Concrete Structures Standard—Part 1: The Design of Concrete Structures Sets out Minimum Requirements for the Design of Reinforced and Pre-Stressed Concrete Structures. Standards New Zealand: Wellington, New Zealand, 2006.
89. *CSA A23.3-04*; Design of Concrete Structures. Canadian Standards Association: Rexdale, TO, Canada, 2004.
90. *AIJ Standard for Structural Calculation of Reinforced Concrete Structures (Japanese)*; Maruzen; Architectural Institute of Japan (AIJ): Tokyo, Japan, 2010.
91. *IS 13920*; Ductile Design and Detailing of Reinforced Concrete Structures Subjected to Seismic Forces-Code of Practice. Bureau of Indian Standards: New Delhi, India, 2016.